The 9th European Congress on Computational Methods in Applied Sciences and Engineering
ECCOMAS Congress 2024
3 – 7 June 2024, Lisboa, Portugal

FINITE ELEMENT ANALYSIS OF BENDING BEHAVIOUR OF GLULAM BEAMS REINFORCED WITH CFRP PLATES

IVAN GLIŠOVIĆ[*], MARIJA TODOROVIĆ[*], NAĐA SIMOVIĆ[*] AND MARKO PAVLOVIĆ[†]

[*] Faculty of Civil Engineering, University of Belgrade
Bulevar kralja Aleksandra 73, 11000 Belgrade, Serbia
e-mail: ivang@grf.bg.ac.rs, todorovicm@grf.bg.ac.rs, nsimovic@grf.bg.ac.rs

[†] Delft University of Technology (TUD)
Mekelweg 5, 2628 CD Delft, Netherlands
email: m.pavlovic@tudelft.nl

Key words: Glulam, CFRP, bending, finite element model, progressive damage.

Summary. Timber structures can effectively be reinforced using externally or internally bonded fibre reinforced polymer (FRP) composites. This paper presents numerical analysis of bending behaviour of glulam beams reinforced with carbon fibre reinforced polymer (CFRP) plates. Nonlinear three-dimensional finite element model was developed and validated by experimental tests carried out on beams with CFRP plates strategically located in the tension zone between the bottom two laminations. Progressive damage model was introduced to effectively tackle the softening behaviour of wood. The numerical results have shown good agreement with the experimental results in relation to load-deflection relationship, ultimate load and stiffness. Nonlinear behaviour of reinforced beams was achieved in the numerical analysis, confirming the finite element model to be accurate past the linear-elastic range.

1 INTRODUCTION

Due to environmental concerns of today's society, timber structures are popular choice in construction industry, as wood represents sustainable and natural material. However, naturality of wood is the reason for heterogeneity and various defects which lower timber mechanical properties. Strengthening or reinforcing timber structures can upgrade mechanical properties or solve various other problems such as mechanical damage, wood defects or increased service load. In this context, development of efficient and suitable reinforcing methodologies is of great importance. Increased availability and affordability of fibre reinforced polymer (FRP) composites have stimulated research and use of these materials in structural applications. Features such as high stiffness and strength, low weight, good durability (no corrosion), electromagnetic neutrality, availability in different shapes and flexibility make FRP composites convenient for timber reinforcement. FRP reinforcement placed in tension zone of timber beams may produce significant improvements in stiffness and ultimate load capacity [1-8].

As experimental research requires resources which make it time-consuming and expensive, numerical models can be cost-effective and time-saving solution. Additionally, numerical

models can be used to further analyse and optimize existing experimentally obtained data. Numerous published works have already numerically investigated performance of FRP reinforced timber members in different arrangements [9-11].

This paper presents numerical analysis of bending behaviour of glulam beams reinforced with carbon fibre reinforced polymer (CFRP) plates strategically located in the tension zone between the bottom two laminations. Nonlinear three-dimensional finite element model was developed using software package Abaqus. Numerical model was validated through comparison of the predicted load-deflection behaviour, stiffness, maximum load and strain profile distribution with experimentally obtained data.

2 EXPERIMENTAL RESEARCH

The experimental research, conducted at the Faculty of Civil Engineering, University of Belgrade, included testing of eight unreinforced beams (Series A) and five beams reinforced with CFRP plates incorporated in between two last laminations of the glulam beams (Series F). The unreinforced beams acted as a control series for reinforced beams. These tests were part of a comprehensive study on reinforcement possibilities of timber beams using FRP materials [6].

2.1 Materials and methods

The glulam beams used for testing were made from spruce timber (*Picea Abies*) classified in the strength class C24 according to EN 338 [12]. Dimensions of the beams were 80 x 210 x 4000 mm, and each beam was composed of seven 30 mm thick laminations. Reinforced beams were manufactured with six laminations, and the seventh one was added in the laboratory after the reinforcement was placed. As reinforcement, unidirectional CFRP plate with a cross section of 1.3 x 60 mm (Sika CarboDur S613) and a length of 4000 mm was used (Figure 1). Mechanical properties of CFRP plate were: modulus of elasticity 165 GPa and tensile strength 2800 MPa [13].

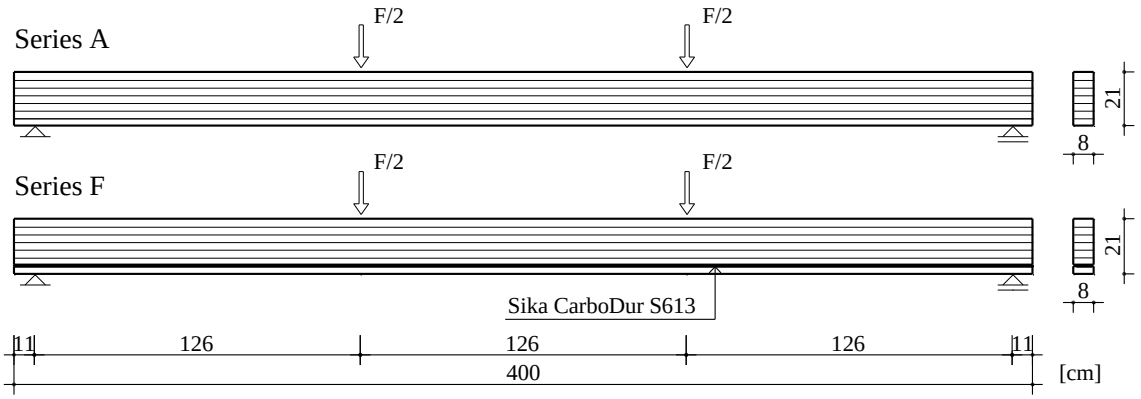

Figure 1: Unreinforced (Series A) and reinforced beam (Series F) test layout

CFRP plate was bonded to the delivered beam consisting of six laminations using epoxy adhesive (Sikadur-330). After proper bond was established between reinforcement and the beam, additional lamination was glued at the bottom. Bonded-in reinforcement is associated with improved fire protection, as well as being visually more acceptable in comparison to

external reinforcement. In addition, possibility of premature delamination is significantly reduced when reinforcement is placed internally due to greater bond area [5].

Testing of all beams was done in accordance with EN 408 [14]. The beams were simply supported over 3780 mm span and tested in four-point bending configuration, as shown in Figure 1. The load was applied using a hydraulic jack at a constant rate of 4.5 kN until failure and it was recorded with a compression load cell. During testing, load was transformed from one load point to two load points using a steel beam. Roller bearings were used as supports and at the load application points. Steel plates were positioned at the load application and support positions to minimize the effects of local indentation. Moreover, lateral bracing was provided to prevent lateral instability of the beams. Deflection at mid-span was measured using linear variable differential transducers (LVDTs). Strains were measured using strain gauges at various locations throughout the beam's height at mid-span. All readings from strain gauges, LVDTs and loading cell were recorded using a computerized data acquisition system.

2.2 Experimental results

Unreinforced glulam beams (Series A) exhibited linear load-deflection behaviour, since failure is caused by excessive tensile stresses in bottom laminations. This failure mode is brittle and sudden without signs of compressive plasticization at the top. Failure was mostly initiated at defects or discontinuities (e.g. knots), which were located in the zone of maximum bending moment between load application points.

Glulam beams reinforced with CFRP plate (Series F) demonstrated significant nonlinear load-deflection behaviour. The most frequent failure mechanism of these beams included two stages: local failure at timber lamination below the reinforcement and global failure above the reinforcement. After the initial linear-elastic behaviour, load resistance dropped sharply due to tensile/bending failure of bottom lamination. As the reinforcement remained in position, the beams continued to carry the load in the same way as beams reinforced at intrados surface (with increased reinforcement percentage) which resulted in nonlinear load-deflection behaviour. Load increased up to a subsequent global tensile/bending failure in laminations above the CFRP plate (Fig. 2a). Compression wrinkles were clearly visible in top laminations (Fig. 2b).

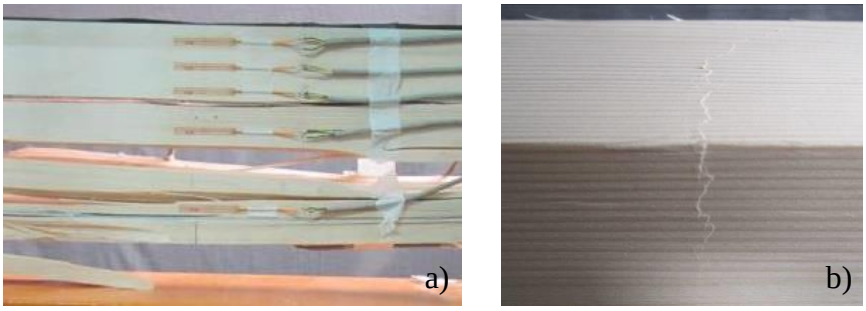

Figure 2: Failure mode of reinforced beams

The results of experimental tests in regard to maximum load, maximum mid-span deflection and bending stiffness are summarized in Table 1. The last column indicates the percentage increase in given values relative to the unreinforced beams. The effect of the reinforcement on the ultimate load-carrying capacity, stiffness and deformability is clearly demonstrated.

Table 1: Experimental results

Test series	Average	Minimum	Maximum	SD	CV (%)	Increase (%)
Maximum load (kN)						
Series A	37.9	32.3	45.4	4.6	12.1	-
Series F	46.4	41.9	52.2	4.3	9.3	22.5
Maximum mid-span deflection (mm)						
Series A	59.9	50.5	66.7	6.0	10.0	-
Series F	95.3	69.3	126.9	24.0	25.2	59.1
Bending stiffness EI ($\times 10^{11}$ Nmm^2)						
Series A	6.46	5.88	7.29	0.50	7.7	-
Series F	7.28	6.70	7.76	0.45	6.2	12.6

SD – Standard deviation, CV – Coefficient of variation

Strain distribution in mid-span across the height was quite linear until failure in the case of unreinforced beams. Tensile and compressive strains were almost identical at different load levels. The position of the neutral axis remained unchanged as the load increased, which proved there was no plasticization in the compression zone.

For the reinforced beams linear strain distribution across the height was observed in the elastic region. Neutral axis moved towards tension zone due to contribution of the CFRP plate. After failure of bottom lamination, neutral axis shifted upwards. No significant variation of neutral axis position was recorded as the applied load increased and plasticization in compression zone occurred. A non-linear strain distribution prior to global failure was noticed.

Table 2 shows average ultimate tensile strains in timber. In addition to improvement in tension strains, strain results demonstrated that timber compressive properties were better utilized when CFRP reinforcement was included in tension zone.

Table 2: Average failure tensile strains in timber

Test series	Tensile strain (‰)	Increase (%)
Series A	3.68	-
Series F	4.52	22.7

3 NUMERICAL MODELLING

3.1 Model description

Using the geometry and test set-up applied in the experimental research, three-dimensional finite element model of unreinforced and reinforced beams was developed in commercial software package Abaqus. In order to optimize calculations and due to the symmetry in geometry, loading and boundary conditions, only 1/4 of beam was modelled while the removed parts were replaced with appropriate symmetry constraints. The end support was considered as a roller support which restrained the beam from movement in the vertical direction. Translation of the beam in the longitudinal direction was permitted as it was in the experimental investigation. The model also included steel plates at loading and support points placed in order to avoid stress concentrations. No slip was included at the interface between steel plates and timber surface. Each lamination was modelled as a separate part with perfect connection

assumed at bonding interfaces between the laminations, since no bond-line failures between laminations were observed during experimental testing. A perfect bonded connection was assumed to exist between timber and reinforcement as bonds of high quality were established during the experimental testing.

Timber was modelled using 8-node solid elements with reduced integration (C3D8R). CFRP plate was modelled using 4-node membrane elements with reduced integration (M3D4R). Steel plates were modelled using 4-node shell elements (S4). A mesh discretisation study was carried out to determine a suitable element size and Figure 3 illustrates finite element mesh. Two finite elements were used through the thickness of each lamination. Finer mesh was generated for laminations adjacent to the CFRP plate, where stress transfer from CFRP plate to glulam occurs.

The numerical analysis was performed using the Dynamic/Explicit solver. A series of vertical displacement increments were applied as a line load over the width of the beam until failure. As geometrical nonlinearities were considered, equilibrium equations are always formulated in the current configuration using current nodal positions, with the update of finite element stiffness matrix at each increment [15].

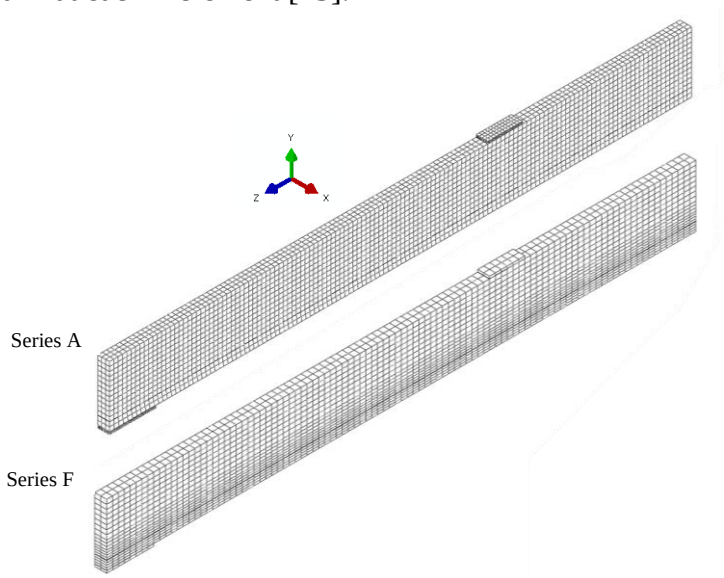

Figure 3: Mesh discretisation for unreinforced (Series A) and reinforced (Series F) beams

3.2 Material characterisation

Suitable constitutive relations for each material were utilised in the model. Three main anatomical directions of wood were assigned to the three principal axes (Figure 4). Nine independent engineering constants (three modulus of elasticity, three shear modulus and three Poisson's ratios) were used to describe the elastic mechanical behaviour of timber. CFRP composite was considered to be a liner-elastic anisotropic material with transverse isotropy. Steel was treated as linear-elastic isotropic material.

Material input parameters for the finite element model were determined from material characterisation testing, known relationships and published data available in the literature. Material properties were assumed to be independent of loading rates. Effects of environment, such as moisture and temperature, on the behaviour of timber were not taken into consideration.

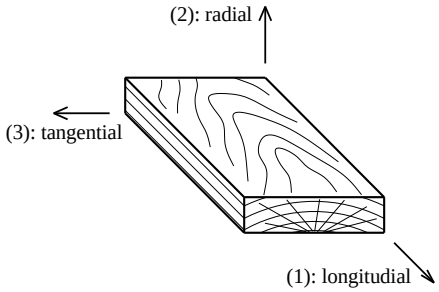

Figure 4: Local coordinate system for timber

The material parameters of timber and CFRP plate used for numerical simulations are presented in Table 3. The modulus of elasticity of timber (E_1) in the longitudinal direction was determined experimentally. Timber has different moduli of elasticity for tension, compression and bending, but their values are very similar and for practical purposes assumed to be identical. General relationships as expressed in [16] were used to calculate the moduli in the transverse directions and shear planes, as well as Poisson's ratios. The elastic parameters for CFRP plate were adopted based on experimental tests (E_1) as well as values given in [17]. The properties in the plate thickness direction were taken the same as those in transverse direction.

Table 3: Material parameters of timber and CFRP plates used in numerical modelling

	Timber	CFRP plate
Modulus of elasticity E (MPa)		
E_1	11,080	165,543
E_2	886	10,000
E_3	554	10,000
Poisson's ratio v (-)		
ν_{12}	0.37	0.3
ν_{13}	0.42	0.3
ν_{23}	0.47	0.03
Shear modulus G (MPa)		
G_{12}	791	5,000
G_{13}	744	5,000
G_{23}	79	1,000

Important part of the numerical procedure is selection of the most adequate timber strength values. Due to stress distribution effect in timber flexural members, tensile stress at failure is greater in bending than in axial tension. Hence, ultimate tensile stress was assumed to be equal to bending strength ($f_{t,0}$ = 42.5 MPa) obtained in bending tests, which were conducted on small timber specimens. The ultimate tensile stress will effectively be increased with addition of CFRP plate. Horizontal reinforcement in tension zone acts as a bridge over timber defects and damages, and contributes to tensile capacity of the beam. Table 2 shows that the average extreme tensile strain at failure increased for reinforced over the unreinforced beams. Large strains at failure indicate large stresses at failure. Since no information was available for tensile strength in bending of reinforced timber, numerical procedure was modified to account for enhancement of bending strength using a modification factor. In this case, according to the ultimate tensile strain data, modification factor was taken as 1.25, therefore $f_{t,0,mod}$ = 53 MPa.

Exponential softening model was used to describe the softening behaviour of wood under tension [18]. For the bottom lamination timber unmodified stress-strain curve was used as the reinforcement had no influence and for laminations above the reinforcement modified stress-strain curve was used, as presented in Figure 5.

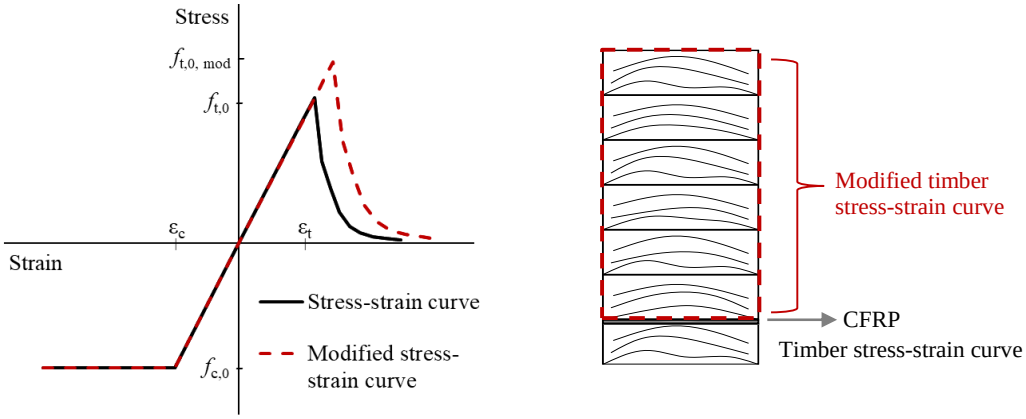

Figure 5: Stress-strain curve for timber

Yield stresses of timber were considered to be equal to its compressive and shear strengths in various directions. These properties were estimated based on conducted material tests and available data for spruce timber in literature. The assumed yield points are shown in Table 4.

Table 4: Yield points assumed for numerical analysis

Yield stress (MPa)							
$\bar{\sigma}_{11}$	$\bar{\sigma}_{22}$	$\bar{\sigma}_{33}$	$\bar{\sigma}_{12}$	$\bar{\sigma}_{13}$	$\bar{\sigma}_{23}$	σ^0	τ^0
36.3	5.0	5.0	6.1	6.1	3.0	36.3	21.0

The theory of anisotropic plasticity was applied to include plastic mechanical behaviour of timber laminations in the compression zone. Plasticity was defined in Abaqus using yield stress and plastic strain. The Hill's criterion for orthotropic materials was used as a condition for transition to the plastic state. Hill's parameters that were used in the model are:

$$R_{11} = \frac{\bar{\sigma}_{11}}{\sigma^0} = \frac{36.3}{36.3} = 1 \qquad R_{12} = \frac{\bar{\sigma}_{12}}{\tau^0} = \frac{6.1}{21.0} = 0.29$$
$$R_{22} = \frac{\bar{\sigma}_{22}}{\sigma^0} = \frac{5.0}{36.3} = 0.14 \qquad R_{13} = \frac{\bar{\sigma}_{13}}{\tau^0} = \frac{6.1}{21.0} = 0.29 \qquad (1)$$
$$R_{33} = \frac{\bar{\sigma}_{33}}{\sigma^0} = \frac{5.0}{36.3} = 0.14 \qquad R_{23} = \frac{\bar{\sigma}_{23}}{\tau^0} = \frac{3.0}{21.0} = 0.14$$

For laminations in tension zone, the progressive damage model was introduced to effectively tackle the softening behaviour of wood. There are eight stress-based failure criteria or damage initiation functions proposed by Sandhaas and van de Kuilen [19]. The tensile failure criterion (Criterion I) was selected to quantify damage initiation and propagation as in the experimental research only tensile failure has occurred. Additionally, based on the observations from the experimental research, only tensile damage in the longitudinal direction of wood was

considered. Therefore, softening behaviour and stiffness degradation in radial and tangential directions were neglected in order to optimize the calculations. The damage initiation and propagation criterion for failure in tension parallel-to-grain can be thus expressed as:

$$F_{t,0}(\sigma) = \sigma_L / f_{t,0} \leq 1 \tag{2}$$

where σ_L - tensile stress parallel-to-grain of damaged material and $f_{t,0}$ - tensile strength.

Once a damage initiation criterion is satisfied, further loading will cause degradation of material stiffness coefficients. Reduction of stiffness coefficients is controlled by damage variables that have values between zero (undamaged state) and one (fully damaged state). Damage variable $d_{t,i}$ is expressed as:

$$d_{t,i} = 1 - \sigma_L / f_{t,0} \tag{3}$$

The evolution of each damage variable in the post-damage initiation phase is governed by an equivalent plastic displacement (Figure 6). The equivalent plastic displacement for a failure mode is expressed as:

$$u_{pl} = L(\varepsilon_{pl} - \varepsilon_{0,pl}) \tag{4}$$

where ε_{pl} - strain of damaged material, $\varepsilon_{0,pl}$ - strain at the onset of damage and L - characteristic length of the finite element.

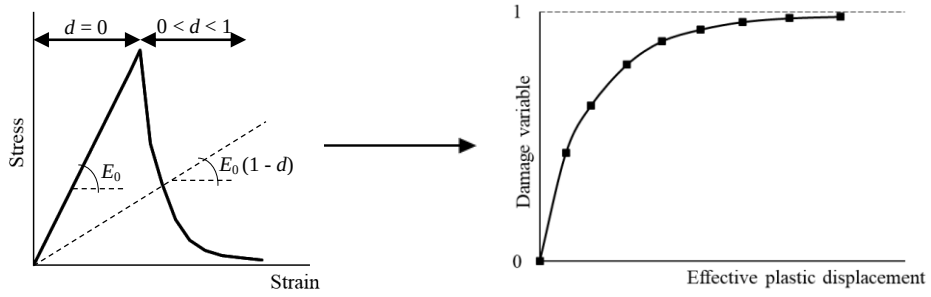

Figure 6: Stress-strain curve transformation to damage variable-effective plastic displacement

It can be seen from Figure 6 that damaged material is implemented as a relation of damage variable d and equivalent plastic displacement u_{pl} in tabular form.

4 RESULTS AND DISCUSSION

Results obtained from the numerical model were verified through the comparison with the test results. The global responses of the beams in terms of load versus mid-span deflection are shown in Figure 7. Based on the presented load-deflection curves, behaviour predicted by the finite element model for unreinforced beams demonstrates good agreement with the experimentally determined behaviour. As it was in the case of experimentally tested unreinforced beams, simulated behaviour was entirely linear elastic up to failure. Developed model of reinforced beams replicated the behaviour of experimentally tested specimens which failed primarily below the reinforcement, with final failure occurring in the lamination above the reinforcement (Figure 8). Once the bottom lamination failed it was excluded from the further analysis and rest of the beam continued carrying the load until the global failure occurred. Nonlinear behaviour of beams before failure was also achieved in the numerical model, confirming the finite element model to be accurate past the linear-elastic range.

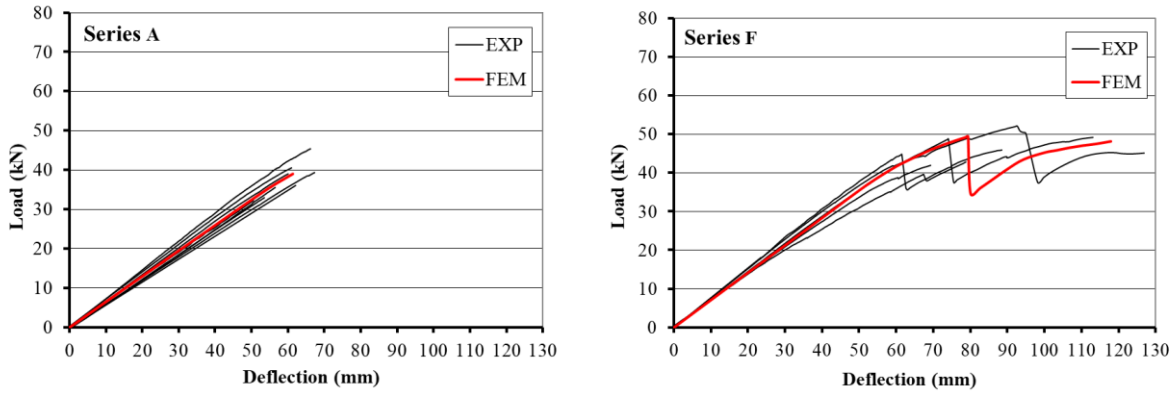

Figure 7: Load-deflection curves for unreinforced (Series A) and reinforced (Series F) beams

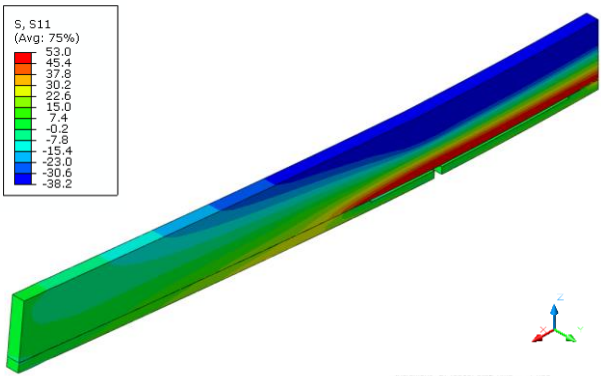

Figure 8: Tensile stress σ_{11} (MPa) at failure for Series F

Ultimate load capacity, deflection at failure and elastic bending stiffness obtained from the model are compared with average experimental results in Table 5.

Table 5: Comparison between experimental results and numerical predictions

Test series	Exp.	FEM	FEM/Exp.
Maximum load (kN)			
A	37.9	39.0	1.029
F	46.4	47.6	1.027
Maximum mid-span deflection (mm)			
A	59.9	61.7	1.030
F	95.3	113.9	1.195
Bending stiffness EI ($\times 10^{11}$ Nmm^2)			
A	6.46	6.53	1.011
F	7.28	7.12	0.978

Numerical and experimental values of load-carrying capacity are very close with a difference of approximately 3% for both unreinforced and reinforced beams. In both cases, the predicted value of the maximum load was higher than the experimental value. Considering the influence of knots and other defects in timber, the error is expected.

The FE model predicted stiffness values agree well with those experimentally determined,

with differences of about 2%. This small deviation proves the uniform quality of the laminations. Given that agreement is strong, it is confirmed that the assumption of perfect adhesion between the CFRP and timber is valid.

The mid-span deflection values show satisfactory compatibility for unreinforced beams. However, the numerical and experimental values of the mid-span deflection at failure show noticeable difference of about 20% for Series F. The cause of this deviation is variability in the experimentally recorded fracture patterns of the beams. If the comparison is made for the average value of the experimental results of beams which showed characteristic behaviour for reinforced beams, the obtained numerical result is somewhat lower than experimental one, with better results agreement (difference of 4.0%).

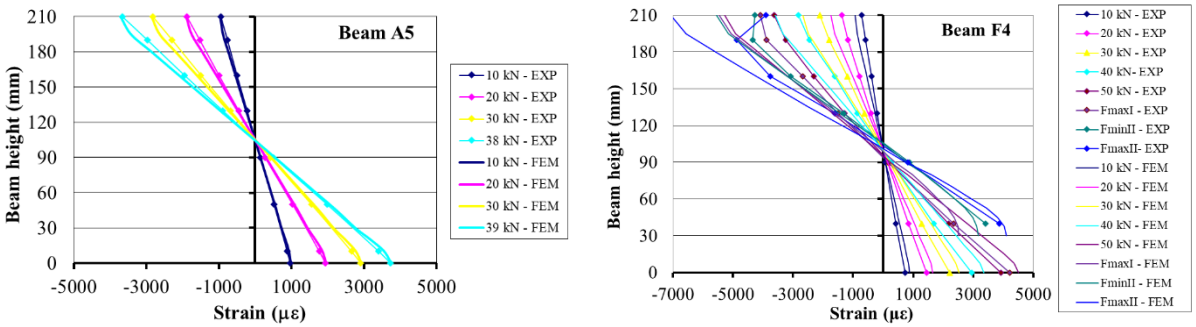

Figure 9: Strain profiles at different load levels for unreinforced (Series A) and reinforced (Series F) beams

The comparisons of experimental and numerical strain profiles at mid-span for different load levels are illustrated in Figure 9. Good agreement of the results is achieved from the simulated strain profiles for both sets of beams. The difference that exists between numerical predictions and experimental values is a result of an average timber modulus of elasticity being used for each lamination, when actually each lamination is inhomogeneous and material properties of timber vary throughout. Also, a reason for deviations in the nonlinear region can be due to the assumption in the numerical analysis that plane sections remain plane after plastic deformation.

5 CONCLUSIONS

Nonlinear finite element model was developed to simulate the bending behaviour of unreinforced and CFRP plate reinforced glulam beams which were previously experimentally tested. Finite element modelling approach was based on elasto-plastic and orthotropic characteristics of timber, Hill's plasticity criterion and progressive damage model to account for softening behaviour of timber. The unreinforced beams demonstrated linear load-deflection behaviour and their dominant failure mode was brittle tensile failure in bottom laminations. The reinforced beams had failure in two stages: local failure at timber lamination below the reinforcement and global failure above the reinforcement, with significant nonlinear load-deflection behaviour. Developed FE models with unique set of parameters simulated the experimentally achieved failure modes for both sets of beams very well. Predictions obtained from the model showed good agreement with the experimental results in terms of load-deflection behaviour, stiffness, ultimate load carrying capacity and strain profile distribution. The proposed numerical methodology can thus be helpful in analysing test results and better understanding of unreinforced and reinforced glulam beams behaviour.

The developed model is easily adjustable to different loading configuration, beam dimensions, material properties and reinforcement percentages. Therefore, it is a valuable tool which can be used to optimise design of timber beams reinforced with FRP plates.

REFERENCES

[1] Raftery, G. M., Harte, A. M. 2011. "Low-grade glued laminated timber reinforced with FRP plate." Composites: Part B, 42(4):724-735. http://dx.doi.org/10.1016/j.compositesb.2011.01.029

[2] Fiorelli, J., Dias A. A. 2011. "Glulam beams reinforced with FRP externally bonded: Theoretical and experimental evaluation." Materials and Structures, 44 (8):1431-1440. https://doi.org/10.1617/s11527-011-9708-y

[3] Kim, Y. J., Hossain, M., Harries K. A. 2013. "CFRP strengthening of timber beams recovered from a 32 year old Quonset: Element and system level tests." Engineering Structures, 57:213-221. https://doi.org/10.1016/j.engstruct.2013.09.028

[4] D'Ambrisi A., Focacci F., Luciano R. 2014. "Experimental investigation on flexural behavior of timber beams repaired with CFRP plates." Composite Structures, 108:720-728. https://doi.org/10.1016/j.compstruct.2013.10.005

[5] Raftery, G. M., Whelan, C. 2014. "Low-grade glued laminated timber beams reinforced using improved arrangements of bonded-in GFRP rods." Construction and Building Materials, 52:209-220. https://doi.org/10.1016/j.conbuildmat.2013.11.044

[6] Glišović, I., Stevanović, B., Todorović, M. 2016. "Flexural reinforcement of glulam beams with CFRP plates." Materials and Structures, 49 (7), pp.2841-2855. https://doi.org/10.1617/s11527-015-0690-7

[7] Yang, H., Lin, W., Lu, W., Zhu S., Geng O. 2016. "Flexural behaviour of FRP and steel reinforced glulam beams: Experimental and theoretical evaluation." Construction and Building Materials, 106:550-563. https://doi.org/10.1016/j.conbuildmat.2015.12.135

[8] Todorović, M., Glišović, I., Stevanović, B. 2022. "Experimental investigation of endnotched glulam beams reinforced with GFRP bars." European Journal of Wood and Wood Products. 80 (5), pp.1071-1085. https://doi.org/10.1007/s00107-022-01822-6

[9] Raftery, G. M., Harte, A. M. 2013. "Nonlinear numerical modelling of FRP reinforced glued laminated timber." Composites: Part B, 52:40-50. https://doi.org/10.1016/j.compositesb.2013.03.038

[10] Nowak, T. P., Jasienko, J., Czepizak, D. 2013. "Experimental tests and numerical analysis of historic bent timber elements reinforced with CFRP strips." Construction and Building Materials, 40:197-206. https://doi.org/10.1016/j.conbuildmat.2012.09.106

[11] Khelifa, M., Auchet,, S., Meausoone P. J., Celzard, A. 2015. "Finite element analysis of flexural strengthening of timber beams with carbon fibre reinforced polymers." Engineering Structures, 101:364-375. https://doi.org/10.1016/j.engstruct.2015.07.046

[12] European Committee for Standardization. 2009. *EN 338: Structural timber - Strength classes.*

[13] Sika CarboDur Plates: Pultruded carbon fiber plates for structural strengthening. Product Data Sheet, Sika AG. www.sika.com

[14] European Committee for Standardization. 2010. *EN 408: Timber structures - Structural timber and glued laminated timber - Determination of some physical and mechanical properties.*

[15] Campilho, R. D. S. G., de Moura, M. F. S. F., Berreto, A. M. J. P., Morais, J. J. L., Domingues, J. J. M. S. 2009. "Fracture behaviour of damaged wood beams repaired with an adhesively-bonded composite patch." Composites: Part A, 40:852-859. https://doi.org/10.1016/j.compositesa.2009.04.007

[16] Bodig, J., Jayne, B. A. 1982. "Mechanics of wood and wood composites." Van Nostrand Reinhold Company, New York.

[17] Harris, B. 1999. "Engineering composite materials." The Institute of Materials, London.

[18] Wang, M., Song, X., Gu, X. 2018. "Three-dimensional combined elastic-plastic and damage model for nonlinear analysis of wood." Journal of Structural Engineering 144(8): 04018103.

[19] Sandhaas, C., van de Kuilen, J.W.G. 2013. "Material model for wood." HERON 58(2/3).